Phenyl-pyta-tricarbonylrhenium(I) complexes: Combining a simplified structure and steric hindrance to modulate the photoluminescence properties

Alexandre Poirot, Corinne Vanucci-Bacqué, Béatrice Delavaux-Nicot, Nadine Leygue, Nathalie Saffon-Merceron, Fabienne Alary, Florence Bedos-Belval, Eric Benoist, Suzanne Fery-Forgues

Phenyl-pyta-tricarbonylrhenium(I) complexes: Combining a simplified structure and steric hindrance to modulate the photoluminescence properties

Alexandre Poirot,[a] Corinne Vanucci-Bacqué,[a] Béatrice Delavaux-Nicot,[b] Nadine Leygue,[a] Nathalie Saffon-Merceron,[c] Fabienne Alary,[d] Florence Bedos-Belval,[a] Eric Benoist [a] and Suzanne Fery-Forgues *[a]

[a] SPCMIB, CNRS UMR 5068, Université de Toulouse III Paul Sabatier, 118 route de Narbonne, 31062 Toulouse cedex 9, France. E-mail : sff@chimie.ups-tlse.fr

[b] Laboratoire de Chimie de Coordination, CNRS (UPR 8241), Université de Toulouse (UPS, INPT), 205 route de Narbonne, 31077 Toulouse Cedex 4, France

[c] Service Diffraction des Rayons X, Institut de Chimie de Toulouse, ICT- UAR 2599, Université de Toulouse III Paul Sabatier, 118 route de Narbonne, 31062 Toulouse cedex 9, France

[d] Laboratoire de Chimie et Physique Quantiques (LCPQ), CNRS UMR 5626, Université de Toulouse III Paul Sabatier, 118 route de Narbonne, 31062 Toulouse cedex 9, France

ABSTRACT

Strongly luminescent tricarbonylrhenium(I) complexes are promising candidates in the field of optical materials. In this study, three new complexes bearing a 3-(2-pyridyl)-1,2,4-triazole (pyta) bidentate ligand with an appended phenyl group were obtained in very good yields owing to an optimized synthetic procedure. The first member of this series, *i.e.* complex **1**, was compared with the previously studied complex **RePBO** to understand the influence of the fluorescent benzoxazole unit grafted on the phenyl ring. Then, to gauge the effect of steric hindrance on the luminescence properties, the phenyl group of complex **1** was substituted in the *para* position by a bulky *tert*-butyl group or an adamantyl moiety, affording complexes **2** and **3**, respectively. The results of theoretical calculations indicated that these complexes were quite similar from an electronic point of view, as evidenced by the electrochemical study. In dichloromethane solution, under excitation in the UV range, all the complexes emitted weak phosphorescence in the red region. In the solid state, they could be excited in the blue region of the visible spectrum and they emitted strong yellow light. The photoluminescence quantum yield was markedly increased with raising the size of the substituent, passing from 0.42 for **1** to 0.59 for **3**. The latter complex also exhibited clear waveguiding properties, unprecedented for rhenium complexes. From this point of view, these easy-synthesized and spectroscopically attractive complexes constitute a new generation of emitters for use in imaging applications and functional materials. However, the comparison with **RePBO** showed that the presence of the benzoxazole group leads to unsurpassed mechanoresponsive luminescence (MRL) properties, due to the involvement of a unique photophysical mechanism that takes place only in this type of complex.

Keywords: Rhenium; Phosphorescence; Crystal; Mechanoresponsive luminescence; DFT; Electrochemical properties

INTRODUCTION

Over the last decade, considerable attention has been paid to the development of luminescent molecules that strongly emit in the solid state and display unconventional behaviours like solid-state luminescence enhancement (SLE) with respect to solutions, and mechanoresponsive luminescence (MRL), i.e. the modification of the emission properties upon grinding, crushing, etc. Transition metal complexes that meet these specifications possess a great potential for practical applications such as chemosensors, bioprobes, stimuli-responsive nanomaterials, and optoelectronic materials.[1] Most of them contain noble metals such as Pt(II), Au(I), Ir(III), Ru(II), Os(IV) and Pd(II), and to a lesser extent Cu(I) and Zn(II). It is therefore of major interest to investigate other types of complexes and to develop a rational design for obtaining materials with efficient and well-controlled luminescence properties.

Owing to their rich photophysical properties, the air- and moisture-stable phosphorescent tricarbonyl rhenium(I) complexes are very attractive light emitters in the solid state. They have been identified for applications as functional materials in the fields of electroluminescence [2,3] solar energy conversion,[4] photocatalysis,[5] and they have emerged as potential thermochromic [6] and photochromic sensors.[7] Some examples of SLE behaviour have been reported, encompassing tetranuclear,[8] dinuclear [9] and mononuclear complexes.[2,10,11] In the last few years, our group has introduced a new family of mononuclear tricarbonyl rhenium(I) complexes incorporating a pyridyl-triazole (pyta) bidentate ligand with appended phenylbenzoxazole (PBO) moiety.[12] Structural optimization allowed complex **RePBO** (Fig. 1) to be selected for its excellent photoluminescence (PL) properties in the solid state.[13] This compound exhibits clear SLE behaviour and was the first reported example of Re(I) complex that displays MRL behaviour.[14] However, the demanding synthesis and purification of **RePBO** may be a drawback for subsequent developments.

Therefore, to overcome this problem while keeping –and even improving- the essential optical properties of **RePBO**, the framework of this complex was simplified and the phenyl functionalization strategy was rethought, as reported in the present work. First, the benzoxazole group was suppressed and replaced by a hydrogen atom, giving complex **1**. Then, it was replaced by two R (*tert*-butyl [15] and adamantyl [16]) bulky groups, affording complexes **2** and **3**, respectively (Fig. 1). These chemical modifications were realized, on the one hand, to clarify the role of the benzoxazole moiety in the PL properties and, on the other hand, to study the impact of steric hindrance on the crystal packing mode and thus on the relevant solid-state emission properties.[17,18] This work shows that one of the new complexes compares well with **RePBO** as regards PL efficiency, and could also lead to Re(I)-based

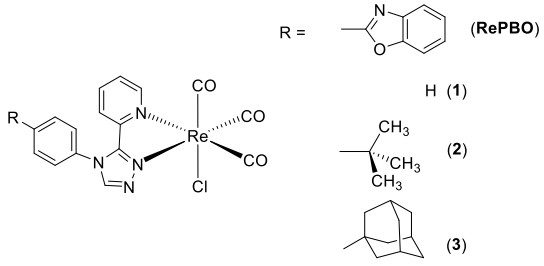

Fig. 1 Chemical structure of the tricarbonyl rhenium(I) complexes

materials with unprecedented optical properties. However, the presence of benzoxazole remains essential for some precise applications.

RESULTS AND DISCUSSION

Synthesis. The access to ligands **L1-L3** was initially envisioned by condensation of aniline derivatives on *N*,*N*-dimethyl-*N'*-picolinoylformohydrazonamide according to a previously described procedure.[13] However, low yield and challenging purification due to presence of many by-products prompted us to develop an alternative strategy. 2-(Pyridin-2-yl)-1,3,4-oxadiazole was initially efficiently synthesized in a one-step procedure by heating pyridine-2-carbohydrazide in triethylorthoformate in the presence of *p*-TsOH (85%).[19] Then, as depicted in Scheme 1, the triazole ligands **L1-L3** were obtained by condensation of the required aniline derivatives (aniline, 4-(*tert*-butyl)aniline and 4-(1-adamantyl)aniline [20]) on 2-(pyridin-2-yl)-1,3,4-oxadiazole in the presence of catalytic *p*-TsOH in refluxing xylenes in good 60-71% yields after purification.[21] Doing so, the overall yield passed from ~30% for the ligand with PBO to >54% for ligands **L1-L3**, with much more reproducible results.

The tricarbonylrhenium(I) complexes **1-3** were then readily obtained by reacting the corresponding ligands with $[Re(CO)_5Cl]$ in refluxing methanol in high yields (90%, 82.5% and 83.2%, respectively). In summary, the improvement of ligand synthesis thus allowed a marked improvement of the whole synthetic process.

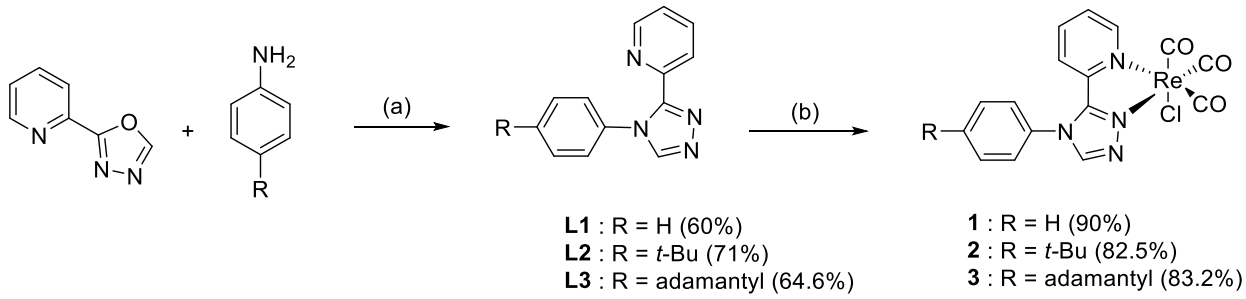

Scheme 1. Synthesis of complexes **1-3**. Conditions and reagents: (a) *p*-TsOH, xylenes, 140°C, 24 h. (b) $[Re(CO)_5Cl]$, MeOH, 65°C, 16 h.

Ligands and complexes were identified by usual methods. The Fourier transform infrared (FTIR) spectra of the four complexes in dichloromethane (DCM) solutions showed the characteristic stretching bands of the three CO groups in a *fac*-$Re(CO)_3$ arrangement. Very close values with average at around 1950 cm^{-1} were found for **1, 2** and **3**, showing that the electron donor ability of the substituted pyta ligand has not significantly varied with substitution.[22] Curiously, it was noticed that the stretching bands of the three complexes were split when using the attenuated total reflectance (ATR) technique on microcrystalline powders (Fig. S1†). The splitting was particularly obvious for **1** and **3**. As this feature was not detected for solutions, it was attributed to an effect of crystallinity.

Crystal structures. X-Ray quality crystals of the three complexes were obtained by slow evaporation of chloroform solutions. Selected crystallographic data are collected in the experimental section (Tables S1 and S2†). Crystals of **2** and **3** are solvates. As expected, the complexes exhibit a slightly-distorted octahedral geometry, in which the rhenium atom is coordinated to three carbonyl groups in a *fac* configuration, one chloride anion and two nitrogen atoms of the pyta ligand (Fig. 2). The coordination sphere presents close bond lengths and angles for the three complexes. The values of the dihedral angle between the triazole and phenyl rings are also very close (68.7(13)° and 67.9(13)° for the two molecules in the asymmetric unit of **1**, 66.8(4)° for **2** and 64.8(4)° for **3**) (Fig. S2†). It is noteworthy that these values are significantly lower than for complex **RePBO**, whose dihedral angle reached 83.30(8)°.[13]

Regarding the crystal packing mode, the three complexes show common features. They form antiparallel dimers (Fig. 3a) well structured by strong interactions between the chlorine atom of one molecule and one hydrogen atom of the pyta group of the other molecule (*i.e.* the H4 of the triazole group for **1** and **2**, the H10 of the pyridyl group for **3**). For the three complexes, the distance between the centers of gravity of two triazole or two pyridyl rings belonging to two distinct molecules is well above 4 Å. Almost no overlap of the aromatic moieties is observed (Fig. S2†). Neighbouring molecules in the stacking direction are distant by more than 3.4 Å. The networks are structured by intermolecular short contacts mainly involving the halogen atom, the carbonyl oxygen atoms and various hydrogen atoms of the organic ligand (Fig. S3†).

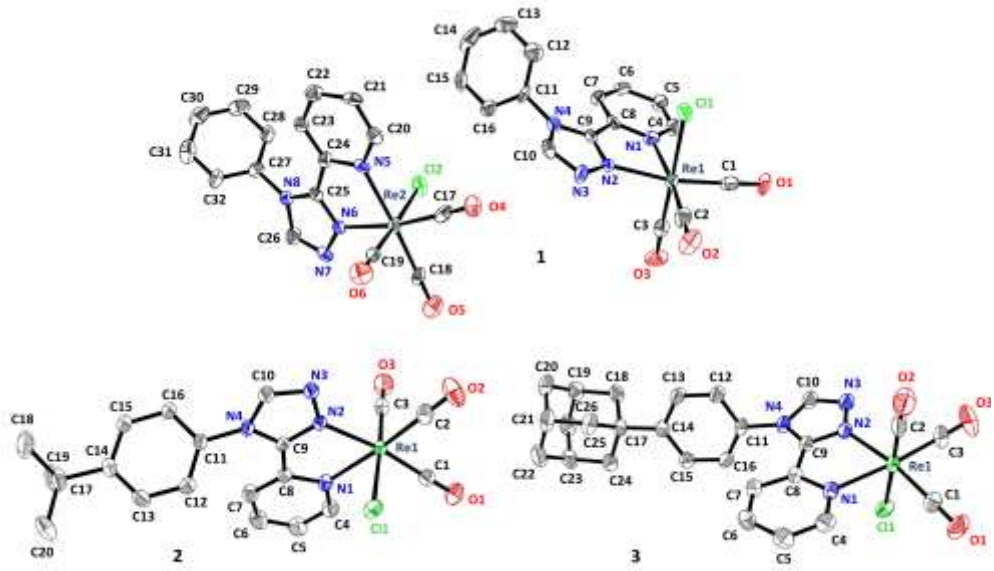

Fig. 2 From top to bottom: Molecular view of the asymmetric unit of complex **1**. Molecular views of complexes **2** and **3.** Hydrogen atoms are not represented for the sake of clarity. Displacement ellipsoids are drawn at 50% probability.

However, the substitution of the phenyl ring also impacts the molecular arrangement (Fig. 3 and S4†). For unsubstituted complex **1**, the pyta motifs of the two types of molecules that constitute the asymmetric unit form almost a right angle (~85.7°). In the network, molecules are densely intertwined. With their moderately bulky *tert*-butyl group, the eight molecules that constitute the unit

cell of complex **2** are displayed along four distinct planes. The *tert*-butyl groups of adjacent molecules interact with each other. The solvent molecules play an important role in separating the complexes. The adamantyl unit of complex **3** brings additional steric constraint. To minimize the neighbouring interactions, the four molecules in the unit cell show two distinct orientations, in which their pyta motifs are almost perpendicular to each other (83.6°). The complexes are separated from each other by both the adamantyl moieties and the solvent molecules. It is noteworthy that the adamantyl moieties have short contacts only with the solvent molecules. Generally speaking, the shortest distance between two rhenium atoms is slightly increased with raising the size of the R substituent (6.42, 7.62 and 7.76 Å for **1**, **2** and **3**, respectively.

By comparison, molecules of **RePBO** have a different packing mode. They form antiparallel dimers with a very small overlap between the benzoxazole unit of one molecule and the pyridyl ring of the neighbouring one, and the dimers are clearly displayed in a herringbone manner.[13]

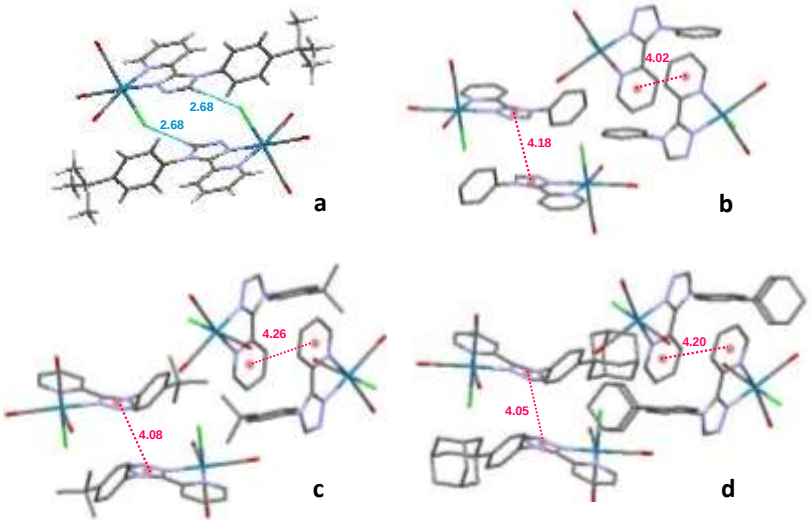

Fig. 3 a) Short Cl-H contacts (in Å) within a dimer formed by two molecules of **2**. Molecular arrangement in crystals of complexes **1** (b), **2** (c) and **3** (d), showing the relative orientation of two pairs of molecules; Hydrogen atoms are omitted for the sake of clarity; the centers of gravity are represented by pink ball.

Electronic structure. Computational studies based on the density functional theory (DFT) method were performed for the complexes in DCM. Since the three complexes were close from an electronic point of view, only the results regarding complex **1** are commented below and illustrated in Fig. 4. The three highest occupied molecular orbitals, i.e. HOMO, HOMO-1 and HOMO-2, were localized on the rhenium atom with contributions of the carbonyl and chloride ligands. In contrast, the electron density of the lowest unoccupied molecular orbitals LUMO and LUMO+1 was mainly localized on the pyta moiety. From the LUMO+2 to the LUMO+5 orbitals, the electron density was distributed between the rhenium carbonyl part and the phenyl ring, and it became preponderant on the latter group with increasing the orbital number. From an energetic viewpoint, the HOMO-LUMO gap of **1** was 4.04 eV.

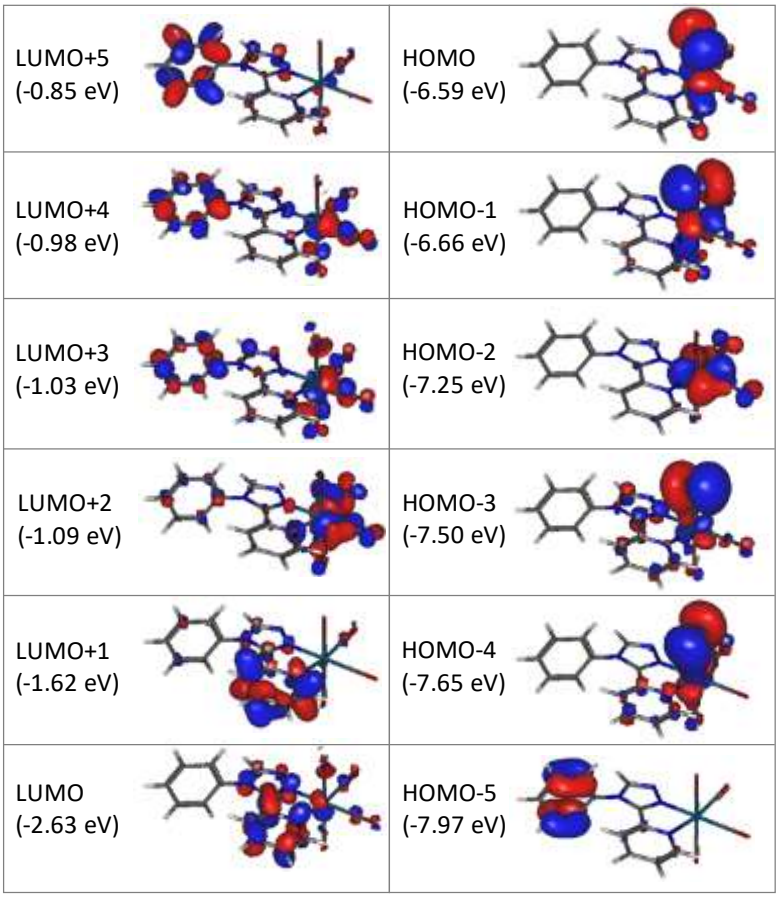

Fig. 4 Energy levels and isodensity plots (isovalue = 0.03) of the first frontier molecular orbitals of complex **1** in dichloromethane, according to DFT calculations at the PBE0/LANL2DZ level of theory.

Electrochemical studies. The electrochemical behaviour of the complexes was studied by cyclic voltammetry (CV) and Osteryoung square wave voltammetry (OSWV) measurements in DCM at room temperature. In the OSWV anodic part, the new complexes were characterized by two oxidation processes at around 1.46 V and 1.77 V, respectively (Table S3†, Fig.S5 to S16†). The former process can be mainly assigned to an irreversible Re(I) oxidation process.[23] This process presents some slightly reversible character when increasing the scan rate around 50 V/s for complexes **2** and **3** (See ESI). Considering the OSWV cathodic part, as for **RePBO**, a clear reduction process was observed for all the new complexes around −1.30 V.[13] It can be attributed to the reduction process of the substituted triazole ring whose value may substantially decrease by complexation as observed in related compounds.[24] As previously proposed, the value of this first reduction process seems to be characteristic of this family of complexes incorporating a 3-(2-pyridyl)-1,2,4-triazole ligand,[12] and could be related to the bent arrangement of the pyta moiety with its connected moiety as illustrated by the X-ray structures. The intensity of the second reduction process around −1.8 V-−1.9 V was much weaker than the first one, or appeared as a shoulder. It was also often ill-defined in CV and situated near the solvent reduction process. In contrast, for **RePBO**, the intensity of the latter process was more important than that of the first one situated at −1.30 V, and it was clearly attributed to the presence of the uncomplexed PBO fragment.[13] In CV, the careful examination of the first reduction process at different scan rates showed that this process becomes quasi-reversible at around 1 V s^{-1} for compounds **1**–**3**. For **RePBO**, the rather uncommon quasi-reversibility of this process implying the

pyta moiety was observed at a lower scan rate, i.e. 0.2 V s^{-1}, suggesting the formation of a more stable one-electron reduction species in solution for the latter compound when compared to the others. Moreover, the three complexes clearly evidenced a 1/1 intensity ratio between the first one-electron reduction process and the first one-electron oxidation process which could be quantified by exhaustive electrolysis of complexes **1** and **2**. The study of this family of complexes by CV (or OSWV) shows at a glance that these compounds have similar electrochemical signatures, close to that of **RePBO** (See for example Fig. 5 and ESI). Consequently, some common electronic properties could be expected for all these complexes, at least in solution. The presence of the adamantyl group on the phenyl moiety of complex **3** leads to the highest first reduction potential, suggesting a slightly highest LUMO level (Table S4†).

The theoretical calculations, which indicate that the HOMOs and LUMOs are mainly located on the metal center and on the pyta moiety, respectively, support our experimental assignments. In addition, the values of the electrochemical HOMO−LUMO gaps (E_g^{el}) [25] of compounds **1**–**3** (2.62 to 2.65 eV) compare well with that of **RePBO** (2.50 eV) under the same conditions, thus indicating that addition of the PBO unit on the phenyl group has only a small influence on this E_g^{el} value. Moreover, these data fit quite well with those of the theoretical study (Table S4†).

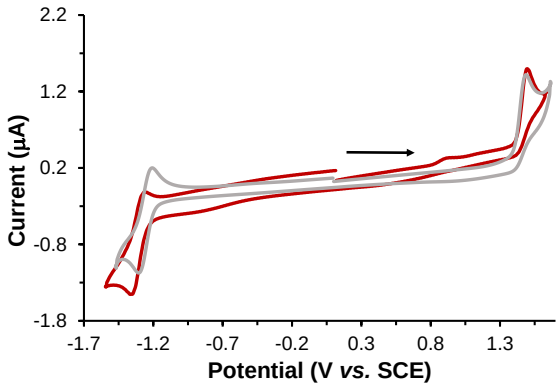

Fig. 5 Cyclic voltammograms of the first oxidation and reduction processes of complexes **3** (red line) and **RePBO** (grey line) in dichloromethane.

Electronic transitions and UV-vis absorption studies. According to TD-DFT calculations, the lowest energy transition associated with high oscillation strength is a HOMO-1→LUMO transition with strong metal to ligand charge transfer (MLCT) character, predicted at 418.2 nm (Fig. S17†, Table S5†). For comparison, the same type of MLCT transition takes place in **RePBO**, where the LUMO is an almost pure π*(pyta) orbital.[13] Around 300-340 nm, all the transitions are of MLCT and ligand to ligand charge transfer (LLCT) nature. The main transition expected at 305 nm involves the HOMO-4 and HOMO-5 orbitals and the LUMO orbital. Finally, many high-energy transitions have LLCT and intra-ligand charge transfer (ILCT) character, and some of them around 250-210 nm involve orbitals located on the phenyl ring.

Regarding now the experimental data (Fig. 6 and Table 1), the absorption spectra in DCM actually showed three bands, shifted to the blue with respect to the predicted values. The weak MLCT band appeared at 382 nm and two intense bands peaked around 282 nm and 238 nm. With respect to **RePBO**, the high-energy bands of **1**–**3** showed a hypsochromic shift by 30-40 nm and their molar

absorption coefficients ε were decreased by more than half, which indicates the reduction of the π-conjugated system of the organic ligand. In contrast, the MLCT bands were at the same wavelength as for **RePBO**, with similar ε value. The reason is probably that, for the two types of complexes, the MLCT band results from the HOMO-1→LUMO transition, with HOMO-1 located on the rhenium center, CO and halogen atom, and the LUMO almost exclusively located on the pyta moiety. Therefore, the phenyl group and its substituent have very small influence.

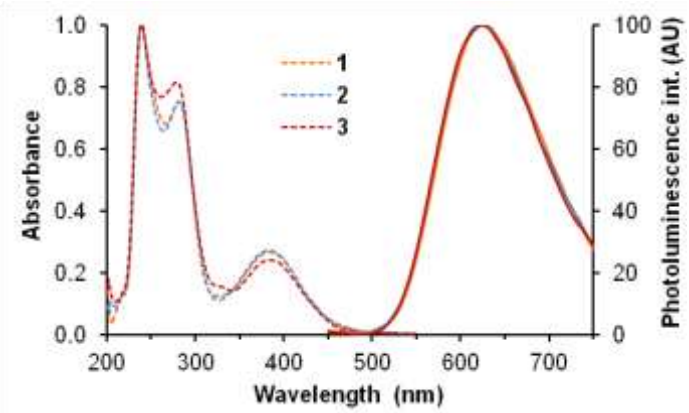

Fig. 6 Normalized UV-vis absorption (dotted lines) and emission spectra (solid lines) of complexes **1** (orange line), **2** (blue line) and **3** (red line) in undegassed dichloromethane. Concentrations ~ 7×10^{-5} M for absorption, ~ 1.8×10^{-5} M for emission. λ_{ex} = 382 nm.

Photochemical stability. Rhenium(I) tricarbonyl complexes that incorporate a diimine ligand and a chloride ligand are known to be photochemically robust, especially in non-coordinating solvents like DCM.[26] Nevertheless, it seemed instructive to check the photochemical behaviour of **1**. A dilute solution in DCM was irradiated at 350 nm in a Rayonet reactor. A very slow evolution of the UV-vis absorption spectrum was observed (Fig. S18†). The photolysis was achieved within 8h. This duration was close to that necessary for the photodegradation of **RePBO** under similar experimental conditions. The identification of the photoproducts will be part of a thorough photochemical study, in comparison with related complexes. Complex **1** was therefore relatively stable from a photochemical point of view. The absence of the benzoxazole moiety does not seem to affect noticeably its lightfastness, while this moiety is generally known to bring photochemical stability to the molecules it is associated with.[27]

Emission properties. When excited by a hand-held UV lamp, DCM solutions of complexes **1**–**3** emitted weak red light. The excitation spectra looked like the absorption spectra. The emission spectra, recorded by exciting at the maximum of the MLCT band, displayed only one unresolved band centered at 626 nm (Table 1 and Fig. 6). Bubbling with argon only led to a small increase of intensity. The emission quantum yields were rather low (~0.02). Luminescence decays were monoexponential and the lifetimes were between 74 and 87 ns, explaining that luminescence was moderately sensitive to the presence of oxygen. The position of the emission spectra at long wavelengths, the lifetimes in the several tens of ns range, and the similarity of these values with those reported for closely related rhenium complexes, allow the emission to be attributed to

phosphorescence. Besides, the maximum wavelength values are in good agreement with the results of DFT calculations for emission arising from the first excited triplet state (606 nm), while fluorescence could be expected at much shorter wavelengths (455 nm) for complex **1**. Remarkably, the emission characteristics of **RePBO** (λ_P = 632 nm, Φ_P = 0.012, τ = 80 ns) [13] were quite close to those of the new complexes.

The microcrystalline powders of **1**–**3** emitted intense yellow light upon excitation by a hand-held UV lamp. Excitation was first performed at 382 nm, like for solutions. However, the excitation spectra of the powders exhibited a distinct band in the blue region of the visible spectrum, with maximum around 470 nm. This was also the case for **RePBO**, although this feature had been unnoticed until now. DFT calculations performed by considering the geometry of complex **1** in the crystal, without allowing any geometrical optimization, led to a theoretical absorption spectrum fairly close to the experimental excitation spectrum (Fig. S20†). Of course, this calculation is only a rough approximation, but our experience shows that it can give some indications about the absorption spectrum of the complex in the crystalline state. This blue band could be the MLCT band, strongly shifted to long wavelengths in the solid state with respect to solutions. Excitation performed at 470 nm resulted in emission spectra exactly superimposable to those obtained by exciting in the UV (see Fig. S21† for an example). Concomitantly, the emission efficiency was decreased by approximately one third, suggesting that intersystem crossing and deexcitation pathways may be different according to the nature of the excited state generated by excitation.[16]

The emission spectra showed only one unresolved band (Fig. 7) with maximum around 550 nm, which reflects well the similarity of the electron conjugated system and intermolecular interactions in the three complexes. The emission decays were monoexponential and the lifetimes were slightly longer for complex **3** (204 ns) than for **1** and **2** (~190 ns). However, the photoluminescence quantum yield (PLQY) was markedly increased from 0.42 to 0.59 with raising the size of the substituent. This difference may be tentatively attributed to the influence of steric hindrance that slightly separates the molecules and may thus reduce some deactivation pathways like the progression of excitons within the crystals and their trapping by crystal defects.[28] With respect to solutions, the solid-state emission was shifted to short wavelengths, the lifetime was significantly longer and the PLQY of the new complexes was multiplied by a factor varying from 21 (complex **1**) to 27 (complex **3**), which indicates a marked solid-state luminescence enhancement (SLE) effect.[28] Such effects are generally attributed to intermolecular interactions and molecular stiffening. Specifically, in the present case, the calculated dihedral angle of complex **1** in the ^{3}MLCT triplet excited state is as wide as 125.2°, while it is only 89.3° in the ground state (Fig. S22†). The optimal geometry of the ^{3}MLCT state is easy to reach when molecules move freely in solution, and emission thus arises from the lowest vibrational levels of the excited state. This is not the case when molecules are embedded in the rigid crystal network, so that emission occurs at higher energy. Besides, the quenching by oxygen and the vibrational modes that favour non-radiative deactivation [14] are reduced for molecules in the solid state compared with solutions, hence the effect on the quantum yields and lifetimes. Finally, it is noticeable that the new complexes emit at slightly longer wavelength, and in the case of **3** with better PL efficiency, than **RePBO** (λ_{PL} = 542 nm, Φ_{PL} = 0.55).[13]

Compounds	Dichloromethane					Solid state								
						Pristine				Ground			THF fumed	
	λ_{abs} [nm]	ε [$M^{-1}cm^{-1}$]	λ_P [nm]	Φ_P	τ [a] [ns] (χ^2)	λ_{ex} [nm]	λ_{PL} [nm]	Φ_{PL}	τ [b] [ns] (χ^2)	λ_{PL} [nm]	Φ_{PL}	τ [b] [ns] (χ^2)	λ_{PL} [nm]	Φ_{PL}
1	240 282 382	15100 11600 4000	626	0.020	74.7 (1.29)	374 472	550	0.42	190 (1.11)	560	0.13	220 (1.21)	550	0.23
2	238 282 382	14500 11600 4100	626	0.022	87.0 (1.20)	374 470	548	0.55	188 (1.07)	558	0.24	219 (1.17)	550	0.45
3	238 282 382	14200 11600 3900	626	0.022	85.6 (1.31)	374 470	550	0.59	204 (1.17)	576	0.11	224 (1.28)	558	0.46
RePBO [c]	310 388	29600 5100	632	0.012	80 (1.19)	372 470	542	0.55	890, f = 0.76 185, f = 0.19	600	0.25	214, f = 0.71 47, f = 0.22	542	0.55

[a] Decays are shown in Fig. S19†.
[b] Acquisition details are commented in the ESI section and in Table S6†.
[c] From ref. 13 and 14, except λ_{ex} of the pristine solid (this work). Excitation at 380 nm. Only the main lifetimes are mentioned.

Table 1 Spectroscopic data of complexes **1**–**3** and **RePBO** in dichloromethane solution and in the solid state. Maximum wavelengths of absorption (λ_{abs}), phosphorescence emission (λ_P), excitation (λ_{ex}) and photoluminescence (λ_{PL}); molar extinction coefficient (ε); phosphorescence and photoluminescence quantum yields (Φ_P and Φ_{PL}); lifetime (τ) and fraction of intensity (f). For solutions, complex concentration ~ 7×10^{-5} M for absorption, ~ 1.8×10^{-5} M for emission. For **1**–**3**, excitation at λ_{ex} = 382 nm for steady-state emission, 370 nm for luminescence decay measurements. For excitation spectra, emission was recorded at the maximum of the emission spectra. All measurements were made at around 20°C.

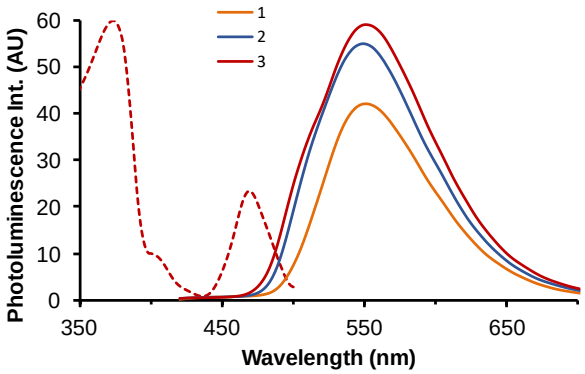

Fig. 7 Excitation spectrum of **3** (λ_{em} = 550 nm, red dotted line) and emission spectra (full lines) of the three complexes **1** (orange line), **2** (blue line) and **3** (red line) as microcrystalline pristine powders. For emission, λ_{ex} = 382 nm and intensity proportional to the PLQY.

The sensitivity of the PL response to mechanical stimuli was then investigated.[29, 30] Upon grinding with a mortar and a pestle, the yellow emission of the four pristine powders slightly turned orange. The emission spectra were shifted to long wavelengths by 10 nm (complexes **1** and **2**) and 26 nm (complex **3**), the PLQY was markedly decreased and the lifetimes became slightly longer (~220 ns). Fuming the samples with tetrahydrofuran vapours generated the strong yellow emission again, although the initial PLQY values were not fully recovered (Table 1). This mechanoresponsive luminescence (MRL) effect was attributed to a switch from crystalline to amorphous phases on the basis of powder X-ray diffraction (pXRD) analysis, as illustrated for **3** in Fig. 8. It can be noticed that the pXRD patterns of the pristine and fumed samples seemed to be slightly different, suggesting a change in crystallinity, which could explain that the MRL effect was not totally reversible for this compound. The spectroscopic effects observed upon grinding can be explained by new intermolecular interactions [30] and by the release of the packing constraints on the molecules, which can thus get closer to the optimal geometry of the ^{3}MLCT triplet excited state (Fig. S22†). The three new complexes behave the same way, and the slight increase in MRL effect observed for **3** may be related to the fact that the packing forces are stronger in complexes **1** and **2** than in **3**, where the molecules are better separated because of steric hindrance. Consequently, grinding could not lead to total amorphization of the first two samples, but rather to a fragmentation into small particles where molecules remain tightly packed. The loose arrangement of the crystal structure of **3** could then favour the MRL effect.

Interestingly, major discrepancies appear when comparing the MLR properties of the new complexeswith those of **RePBO**. First of all, the MRL phenomenon was much weaker for complexes **1**–**3** than for **RePBO**, the emission spectrum of which was red-shifted by 58 nm to long wavelengths upon grinding. Additionally, the pristine powder of **RePBO** shows two main decays, *i.e.* one of minor contribution with a lifetime at 185 nm comparable to that of complexes **1**–**3**, and a very predominant decay with lifetime at 890 nm, totally absent in the new complexes. After grinding the **RePBO** powder, the long lifetime disappears, and the emitting species has a lifetime of 215 ns, just like in complexes **1**–**3**.

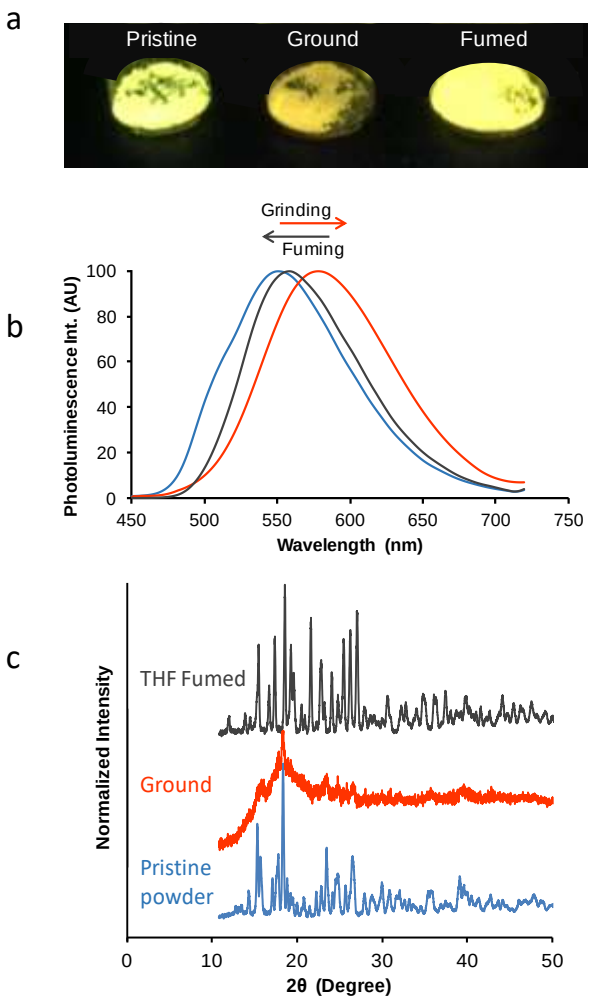

Fig. 8 a) Image of the microcrystalline powders of complex **3** before and after grinding, and after THF fuming, upon illumination by a UV lamp (365 nm). b) Normalized photoluminescence spectra of the pristine (blue line), ground (red line) and THF-fumed (grey line) samples of **3**, λ_{ex} = 382 nm. c) Corresponding pXRD patterns.

These different behaviours may be explained as follows. In our previous work on **RePBO**, the MRL effect was shown to arise from the interplay between two low-lying triplet excited states with very close energy levels (Fig. 9a).[14] Our hypothesis was that a triplet excited state having almost pure intraligand (IL) character is responsible from the yellow light and long lifetime that predominate in the emission of pristine microcrystals. In turn, the ^{3}MLCT triplet excited state gives the orange emission and short lifetime mainly observed in the amorphous phase. Transition between these two states is promoted by rotation around the pyta-PBO bond, occurring more easily in the amorphous phase than in crystals. At the opposite, for complexes **1**–**3**, DFT calculations did not allow identifying any low-lying triplet excited state other than the ^{3}MLCT state, which is therefore fully responsible for emission in both the microcrystalline and amorphous phases. The small spectroscopic variations observed between these phases would be due only to different molecular environment and geometrical constraints.[30]

A glance at the energy levels helps better understand the photophysical processes that take place in our compounds. The ^{3}MLCT triplet excited state is probably very similar for both types of

complexes. For **1**−**3**, its orbitals are precisely located around the coordination sphere of the rhenium, with almost no involvement of the phenyl ring (Fig. S23†). It is also the case for **RePBO**, where the benzoxazole moiety, situated beyond the phenyl group, plays a weak role in the phosphorescence emission in solution. The presence of benzoxazole only leads to a weak decrease of the energy level of the ^{3}MLCT triplet excited state, testified by the small red-shift of the emission spectrum in solution. In contrast, the orbitals of the ^{3}IL triplet excited state of **RePBO** extend on the whole PBO moiety, quite a large delocalized electron system that does not exist in complexes **1**−**3**. Whatever their nature, triplet excited states other than the ^{3}MLCT state are probably at much higher energy in **1**−**3** than in **RePBO**. In this case, the low-lying ^{3}MLCT state is greatly populated and totally responsible for emission of **1**−**3** in the solid phases. The comparison of the radiative processes occurring in **RePBO** and in complexes **1**−**3** is proposed in Fig. 9.

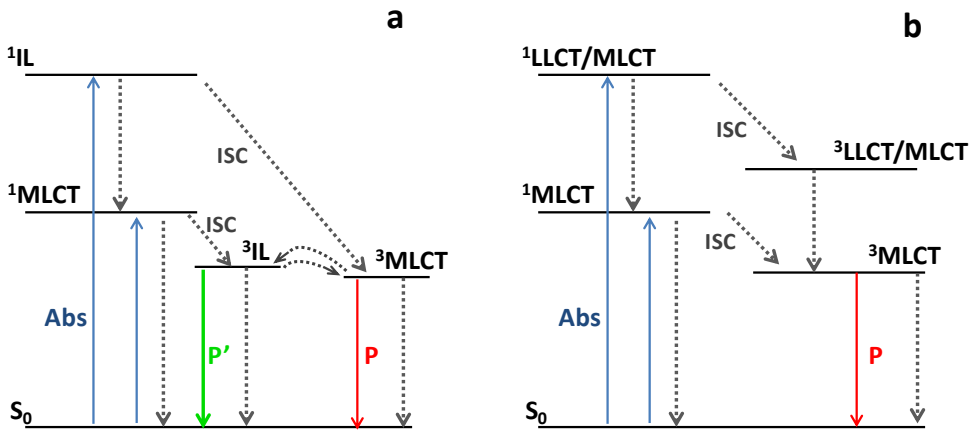

Fig. 9 Schematized photoluminescence processes in the two types of complexes. a) For **RePBO**, photoluminescence emission P' is preponderant in crystals while P takes place in the amorphous phase and in solution. b) For complexes **1**−**3**, only photoluminescence P is observed in every case**.** Only the main radiative (solid lines) and non-radiative (dotted lines) transitions occurring between the ground state and first excited states are represented. High energy excited states are omitted. Abs: absorption; P: phosphorescence; ISC: intersystem crossing.

Finally, microcrystals of complexes **1**–**3** have been observed under the fluorescence microscope. Of course, all of them emitted strong yellow light (Fig. 10 and S24†). A self-waveguided edge-emission effect was particularly clear for the large platelets of **3** grown from chloroform solutions, the surface of which appeared dark, while a strong light was emitted by the edges. According to the literature, this effect is characteristic of a particular alignment of the transition dipoles in the crystal.[31]

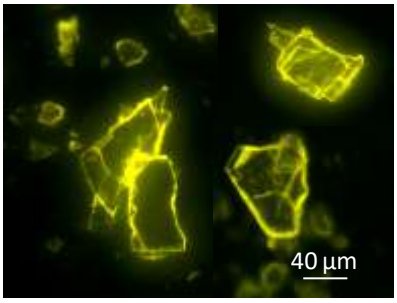

Fig. 10 Fluorescence microscopy image of crystals of complex **3** (λ_{ex} ~ 450−490, λ_{em} > 500 nm).

CONCLUSIONS

Owing to its astounding spectroscopic properties in the solid state, **RePBO** was introduced as the prototype of a new generation of tricarbonylrhenium(I) complexes. The present study showed that new benzoxazole-free counterparts are easier to prepare. Indeed, the optimization of the synthetic procedure of the three new ligands allowed complexes **1**–**3** to be obtained with good yields. The absence of the benzoxazole moiety in **1**–**3** had little effect on the electrochemical and spectroscopic properties in solution. In the solid state, the colour of the emitted light remained the same, but the presence of a bulky substituent was necessary to obtain PLQY equal to, or even greater than that of **RePBO**. This high PLQY, together with the good photochemical stability and possible excitation in the visible range, make the adamantyl-substituted complex **3** an attractive candidate for applications in the field of photonic materials. From this perspective, this complex could favourably compete with recently reported room-temperature phosphorescence (RTP) organic materials.[32] It also showed clear waveguiding properties, which, to the best of our knowledge, have not been reported for rhenium complexes so far. Generally speaking, taking advantage of the easy synthesis and attractive properties of complexes **1**–**3**, various derivatives are presently under study with the aim to access new luminescent materials and bioconjugates for SLE-based bio-imaging applications, such as the monitoring of aggregation processes.

However, the MRL properties of **RePBO** were unsurpassed, due to a major change in the photophysical processe of emission between the two types of complexes. This observation highlights the value of the PBO moiety for all applications linked with MLR properties, and open the way to further developments in this field.

EXPERIMENTAL SECTION

General methods. All purchased chemicals were of the highest purity commercially available and used without further purification. Analytical grade solvents were used as received. Unless otherwise noted, all reactions were carried out under a nitrogen atmosphere. They were monitored by TLC on silica gel Alugram® Xtra SIL G/UV_{254}. Column chromatography was performed on Machery-Nagel silica gel or neutral alumina.

NMR, mass and infrared spectra were obtained in the relevant ‘Services communs de l’Institut de Chimie de Toulouse, Université de Toulouse III Paul-Sabatier’. ^{1}H- and ^{13}C-NMR spectra were recorded on a Bruker Avance 300 MHz spectrometer. Attributions of the signals were made using 2D NMR data (COSY, HSQC and HMBC). Protons and carbon atoms were numbered according to Fig. S25†. Signals are described as follow: s, singlet; d, doublet; t, triplet; m, multiplet. App = Apparent; * = The multiplicity of the signal is more complex as it is part of an AAXX system. All spectra are given in Fig. Fig. S26†. HRMS data were recorded on a Xevo G2 QTOF (Waters) instrument. Infrared spectra were obtained on a Nexus Thermonicolet apparatus with DTGS as the detector. Microanalyses were made in the ‘Service d’analyses’ of LCC using a Perkin Elmer 2400 series II analyzer. Melting points (Mp) were obtained on a Buchi apparatus and are uncorrected. Measurements above 200°C

were not possible with this apparatus. Fluorescence microscopy was performed with a Leitz Laborlux D fluorescence microscope equipped with an Andor Luca camera.

2-(Pyridin-2-yl)-1,3,4-oxadiazole. A mixture of pyridine-2-carbohydrazide (3 g, 21.9 mmol) and *p*-TsOH (330 mg, 1.73 mmol) in triethylorthoformate (15 mL) was heated at 130°C for 6h. After cooling to room temperature, part of the expected product spontaneously precipitated and was collected by filtration. Water was added to the filtrate and the aqueous layer was extracted with EtOAc. The combined organic layer was dried over Na_2SO_4, concentrated under reduced pressure, and the residue was purified by recrystallization from EtOH. The gathering of the precipitated and recrystallized products afforded the expected oxadiazole as a white solid (2.77 g, 85%). Mp = 119.5°C (litt. [ref. 19] = 115°C). ^{1}H NMR (300 MHz, $CDCl_3$): δ (ppm) = 8.79 (ddd, *J* = 4.9, 1.8, 0.9 Hz, 1H); 8.57 (s, 1H); 8.29 (dt, *J* = 7.9, 1.1 Hz, 1H); 7.91 (td, *J* = 7.7, 1.8 Hz, 1H); 7.49 (ddd, *J* =7.7, 4.9, 1.2 Hz, 1H). ^{13}C NMR (75 MHz, $CDCl_3$): δ (ppm) = 163.9; 153.5; 150.3; 143.14; 137.3; 126.1; 123.4.

General procedure for the preparation of ligands L1-L3.
To a solution of 2-(pyridin-2-yl)-1,3,4-oxadiazole (1 mmol) in xylene (3 mL) were added the requisite aniline derivative (1 mmol) and *p*-TsOH (0.1 mmol). The reaction mixture was stirred under nitrogen atmosphere at 140°C for 24h. After cooling to room temperature, EtOAc was added and the organic layer was washed with 1M aqueous NaOH solution (10 mL), dried over Na_2SO_4 and concentrated under reduced pressure. Column chromatography afforded the pure expected compound.

2-(4-phenyl-4H-1,2,4-triazol-3-yl)pyridine (L1). Following the general procedure, 294 mg of oxadiazole (2 mmol) and 186 mg (2 mmol) of aniline afforded triazole **L1** (266 mg, 60%) as a white solid after column chromatography (alumina, CH_2Cl_2/PE = 8:2 to 9:1). ^{1}H NMR (300 MHz, $CDCl_3$): δ (ppm) = 8.41–8.34 (m, 2H, $H_{1\text{-}7}$); 8.17 (dt, *J* = 7.9, 1.1 Hz, 1H, H_4,); 7.82 (td, *J* = 7.8, 1.8 Hz, 1H, H_3); 7.53–7.43 (m, 3H, $H_{9\text{-}11}$); 7.37–7.23 (m, 3H, $H_{2\text{-}10}$). ^{13}C NMR (75 MHz, $CDCl_3$) δ (ppm)= 152.2; 149.1; 146.7; 145.7; 136.9; 135.4; 129.4; 129.1; 126.0; 124.3; 124.1. HRMS (ESI+) *m/z* 223.0980 ($[M+H]^+$ calcd for $C_{13}H_{11}N_4$: 223.0984).

2-(4-(4-(*tert*-Butyl)phenyl)-4H-1,2,4-triazol-3-yl)pyridine (L2). Following the general procedure, 147 mg of oxadiazole (1 mmol) and 160 µL (1 mmol) of 4-(*tert*-butyl)aniline afforded triazole **L2** (196 mg, 71%) as a white solid after column chromatography (silica gel, EtOAc). Mp = 109–111°C. ^{1}H NMR (300 MHz, $CDCl_3$): δ (ppm) = 8.40 (ddd, *J* = 4.9, 1.8, 1.0 Hz, 1H, H_1); 8.32 (s, 1H, H_7); 8.12 (dt, *J* = 7.9, 1.1 Hz, 1H, H_4); 7.79 (td, *J* = 7.8, 1.8 Hz, 1H, H_3); 7.44 (app d*, *J* = 8.6 Hz, 2H, H_{10}); 7.27-7.24 (m, 1H, H_2); 7.20 (app d*, J = 8.7 Hz, 2H, H_9); 1.36 (s, 9H, *t*-Bu). ^{13}C NMR (75 MHz, $CDCl_3$): δ (ppm) = 152.2; 152.1; 149.1; 146.7; 145.7; 136.8; 132.6; 127.2; 125.3; 124.12; 124.07; 33.8; 31.3. HRMS (DCI/CH_4) *m/z* 279.1599 ($[M+H]^+$ calcd for $C_{17}H_{19}N_4$: 279.1610).

2-(4-(4-((3r,5r,7r)-Adamantan-1-yl)phenyl)-4H-1,2,4-triazol-3-yl)pyridine (L3).
Following the general procedure, 147 mg of oxadiazole (1 mmol) and 228 mg (1 mmol) of 4-(1-adamantyl)aniline afforded triazole **L3** (230 mg, 64.6%) as a white solid after column chromatography (silica gel, (EtOAc/CH_2Cl_2 =1:1). Mp > 220°C. ^{1}H NMR (300 MHz, $CDCl_3$): δ (ppm) = 8.39 (ddd, *J* = 4.9, 1.8, 0.9 Hz, 1H, H_1); 8.32 (s, 1H, H_7); 8.11 (dt, *J* = 7.9, 1.1 Hz, 1H, H_4) ; 7.78 (td, *J* = 7.8, 1.8 Hz,

1H, H_3) ; 7.41 (app d*, *J* = 8.7 Hz, 2H, H_{10}); 7.26 (m, 1H, H_2); 7.20 (app d*, *J* = 8.7 Hz, 2H, H_9); 2.12 (m, 3H, H_{14}); 1.93 (m, 6H, H_{13}); 1.84-1.79 (m, 6H, H_{15}). ^{13}C NMR (75 MHz, $CDCl_3$): δ (ppm) = 152.3; 152.2; 149.1; 146.7; 145.7; 136.7; 132.5; 125.8; 125.3; 124.1; 124.0; 43.0; 36.6; 36.2; 28.8. HRMS (DCI/CH_4) *m/z* 357.2079 ($[M+H]^+$ calcd for $C_{23}H_{25}N_4$: 357.2079).

General procedure for the preparation of tricarbonylrhenium(I) complexes 1-3.
A mixture of the ligand and $[Re(CO)_5Cl]$ (1.05–1.1 eq.) in methanol was stirred for 16h at 65 °C. The reaction mixture was cooled to room temperature and the yellow precipitate was collected by filtration, washed with methanol and dried *in vacuo*. The expected product was pure enough to be used without further purification.

Complex $[Re(CO)_3(L1)Cl]$, 1. Following the general procedure, 31.7 mg (0.142 mmol) of **L1** and 54.05 mg (0.150 mmol) of $[Re(CO)_5Cl]$ afforded complex **1** (68 mg, 90%) as a yellow solid. ^{1}H NMR (300 MHz, $CDCl_3$): δ (ppm) = 9.13 (ddd, *J* = 5.5, 1.6, 0.8 Hz, 1H, H_1); 8.34 (s, 1H, H_7); 7.77 (m, 4H, $H_{3\text{-}10\text{-}11}$), 7.57 (d, *J* = 7.3 Hz, 2H, H_9), 7.51(ddd, *J* = 7.8, 5.5, 1.3 Hz, 1H, H_2); 7.04 (dt, *J* = 8.0, 1.1 Hz, 1H, H_4,). ^{13}C NMR (75 MHz $CDCl_3$): δ (ppm) = 197.3; 195.4; 188.3; 154.9; 154.6; 146.4 (C_7); 144.9; 138.9 (C_3); 132.4; 132.2; 131.3; 127.7; 126.8; 122.7. HRMS (ESI) *m/z* 550.9897 ($[M+Na]^+$ calcd for $C_{16}H_{10}N_4O_3NaCl^{185}Re$: 550.9897). IR ($CH_2Cl_2$): ν(CO) = 2027, 1926, 1897 cm^{-1}. Anal. calcd (%) for $C_{16}H_{10}N_4O_3ReCl$: C 36.40, H 1.91, N 10.61; found: C 36.22, H 1.96, N 10.43.

Complex $[Re(CO)_3(L2)Cl]$, 2. Following the general procedure, 186 mg (0.658 mmol) of L2 and 266 mg (0.735 mmol) of $[Re(CO)_5Cl]$ afforded complex **2** as a yellow solid. (322 mg, 82.5%). ^{1}H NMR (300 MHz, $CDCl_3$): δ (ppm) = 9.13 (ddd, *J* = 5.5, 1.5, 0.8 Hz, 1H, H_1); 8.28 (s, 1H, H_7); 7.81 (td, *J* = 7.9, 1.6 Hz, 1H, H_3); 7.71 (app d*, *J* = 8.8 Hz, 2H, H_{10}); 7.52-7.47 (m, 1H, H_2); 7.46 (app d*, *J* = 8.7 Hz, 2H, H_9); 7.10 (ddd, *J* = 8.1, 1.3, 0.9 Hz, 1H, H_4); 1.44 (s, 9H, *t*-Bu). ^{13}C NMR (75 MHz, DMSO-d_6): δ (ppm) = 197.8; 197.2; 189.0; 154.6; 154.3; 154.2; 148.5 (C_7); 143.6; 140.5; 129.7; 128.2; 127.4; 126.5; 122.6; 33.6 ($Cq_{\text{t-Bu}}$); 31.0 (CH_3). HRMS (ESI) *m/z* 605.0485 ($[M+Na]^+$ calcd for $C_{20}H_{18}N_4O_3NaCl^{185}Re$: 605.0495), *m/z* 547.0905 ($[M-Cl]^+$ calcd for $C_{20}H_{18}N_4O_3{}^{185}Re$: 547.0908). IR ($CH_2Cl_2$): ν(CO) = 2027, 1926, 1897 cm^{-1}. Anal. calcd (%) for $C_{20}H_{18}N_4O_3ReCl$: C 41.13, H 3.11, N 9.59; found: C 41.01, H 2.96, N 9.47.

Complex $[Re(CO)_3(L3)Cl]$, 3. Following the general procedure, 200 mg (0.651 mmol) of **L3** and 223 mg (0.616 mmol) of $[Re(CO)_5Cl]$ afforded complex **3** as a yellow solid. (308 mg, 83.2%). ^{1}H NMR (300 MHz, $CDCl_3$): δ (ppm) = 9.12 (dt, *J* = 5.1, 1.3 Hz, 1H, H_1); 8.29 (s, 1H, H_7); 7.80 (td, *J* = 7.9, 1.5 Hz, 1H, H_3); 7.68 (app d*, *J* = 8.7 Hz, 2H, H_{10}); 7.52-7.48 (m, 1H, H_2); 7.47 (app d*, *J* = 8.6 Hz, 2H, H_9); 7.09 (dd, *J* = 8.0, 1.0 Hz, 1H, H_4); 2.19 (m, 3H, H_{14}); 2.00 (m, 6H, H_{13}); 1.89-1.77 (m, 6H, H_{15}). ^{13}C NMR (75 MHz, DMSO-d_6): δ (ppm) = 197.8; 197.2; 189.0; 154.5; 154.4; 154.3; 148.1 (C_7); 144.2.; 140.5; 129.6; 128.2; 126.9; 126.5; 122.6; 42.3; 36.2; 36.0; 28.2. HRMS (ESI) *m/z* 683.0956 ($[M+Na]^+$ calcd for $C_{26}H_{24}N_4O_3NaCl^{185}Re$: 683.0964), *m/z* 625.1370 ($[M-Cl]^+$ calcd for $C_{26}H_{24}N_4O_3{}^{185}Re$: 625.1378). IR ($CH_2Cl_2$): ν(CO) = 2027, 1926, 1897 cm^{-1}. Anal. calcd (%) for $C_{26}H_{24}N_4O_3ReCl$: C 47.16, H 3.65, N 8.46; found: C 47.22, H 3.60, N 8.29.

X-ray crystallography. Crystal data were collected at 193K using MoKα radiation (wavelength = 0.71073 Å) on a Bruker AXS Quazar APEX II diffractometer using a 30 W air-cooled microfocus source (ImS) with focusing multilayer optics (**1** and **2**) and on a Bruker-AXS D8-Venture diffractometer equipped with a Photon III-C14 detector (**3**). Phi- and omega-scans were used. Space group was determined on the basis of systematic absences and intensity statistics. Semi-empirical absorption correction was employed.[33] The structures were solved using an intrinsic phasing method (ShelXT).[34] All non-hydrogen atoms were refined anisotropically using the least-square method on F^2.[35] Hydrogen atoms were refined isotropically at calculated positions using a riding model with their isotropic displacement parameters constrained to be equal to 1.5 times the equivalent isotropic displacement parameters of their pivot atoms for terminal sp3 carbon and 1.2 times for all other carbon atoms. In structure **3**, the solvent (chloroform) was disordered over two or three positions: several restraints (SAME, SIMU, DELU, ISOR) were applied to refine some moieties of the molecules and to avoid the collapse of the structures during the least-squares refinement by the large anisotropic displacement parameters. Selected crystallographic data are collected in Table 2.

	1	**2**	**3**
Empirical formula	$C_{16}H_{10}ClN_4O_3Re$	$C_{20}H_{18}ClN_4O_3Re,CHCl_3$	$C_{26}H_{24}ClN_4O_3Re$, $CHCl_3$
Formula weight	527.94	703.40	781.51
Crystal system	Triclinic	Orthorhombic	Monoclinic
Space group	$P\ \bar{1}$	Pbca	$P2_1/n$
Unit cell dimensions			
a (Å)	10.8275(13)	10.9645(7)	16.9598(9)
b (Å)	12.8483(16)	18.8237(11)	10.7879(5)
c (Å)	13.1018(18)	25.0238(15)	17.1754(8)
α (°)	89.948(4)	90	90
β (°)	76.460(4)	90	112.3536(18)
γ (°)	73.825(4)	90	90
Volume ($Å^3$)	1697.8(4)	5164.7(5)	2906.3(2)
Z	4	8	4
Density (calculated) (Mg/m^3)	2.065	1.809	1.786
Crystal size (mm^3)	0.020 × 0.020 × 0.060	0.200 × 0.120 × 0.040	0.200 × 0.200 × 0.100
Reflections collected	35952	165560	145772
Independent reflections	6908	8050	7201
R_{int}	0.1083	0.0665	0.0329
Restraints/parameters	12/451	0/301	360/427
Final R1 index I>2σ(I)	0.0435	0.0284	0.0239
wR2 (all data)	0.0901	0.0561	0.0700
Largest diff. peak and hole (e $Å^{-3}$)	1.264 and -1.657	1.323 and -1.303	1.026 and -1.138
CCDC	2089469	2089470	2089471

Table 2. Selected crystallographic data of complexes **1**, **2** and **3**.

The powder X-ray diffraction patterns were recorded in the "Nano X platform of CEMES-CNRS". The powders were placed in a sample holder with no background noise. The measurements were made in reflection mode using a Bragg-Brentano configuration on a Bruker D8 Advance diffractometer equipped with a Copper anticathode (Cu Kα1 = 1.54059 Å and Kα2 = 1.54439 Å) and a 1D Lynx eye detector.

Electrochemistry. The electrochemical properties of the new compounds were determined by cyclic voltammetry (CV) and Osteryoung square wave voltammetry (OSWV) in DCM. The solutions

used during the electrochemical studies were typically 1×10^{-3} M in complex, and 0.1 M in supporting electrolyte. The supporting electrolyte (nBu$_4$N)(BF$_4$) (Fluka, 99% electrochemical grade) was used as received and simply degassed under Ar. DCM was dried using an MB SPS-800 solvent purification system just prior to use. The measurements were carried out with an Autolab PGSTAT100 potentiostat controlled by GPES 4.09 software. Experiments were performed at room temperature (r.t.) in a homemade airtight three-electrode cell connected to a vacuum/Ar line. The reference electrode consisted of a saturated calomel electrode (SCE) separated from the solution by a bridge compartment. The counter electrode was a Pt wire of ca. 1 cm^2 apparent surface. The working electrode was a Pt microdisk (0.5 mm diameter). Before each measurement, the solutions were degassed by bubbling Ar and the working electrode was polished with a polishing machine (Presi P230). Under these experimental conditions, Fc^+/Fc is observed at +0.55 ± 0.01 V *vs*. SCE. OSWVs were obtained using an amplitude of 20 mV, a frequency of 20 Hz, and a step potential of 5 mV.

Spectroscopy and photochemistry. Spectroscopic measurements in solutions were conducted at 20°C in a temperature-controlled cell. UV-visible absorption spectra and emission spectra in solutions were measured with a Xenius SAFAS spectrofluorometer using cells of 1 cm optical pathway. All emission spectra were corrected. The emission quantum yields in solution (Φ_F) were determined using the classical formula: $\Phi_x = (A_s \times F_x \times n_x^2 \times \Phi_s)/(A_x \times F_s \times n_s^2)$ where A is the absorbance at the excitation wavelength, F the area under the fluorescence curve and n the refraction index. Subscripts s and x refer to the standard and to the sample of unknown quantum yield, respectively. Coumarin 153 (Fluorescence Φ_F = 0.53) in ethanol was used as the standard.[36] The absorbance of the solutions was equal or below 0.06 at the excitation wavelength. The error on the emission quantum yield values is estimated to be about 10 %.

Solid state spectra were recorded on the same Xenius SAFAS spectrofluorometer equipped with an integrating sphere and corrected using a home-made correction curve. Solid samples were deposited on a metal support. The absolute photoluminescence quantum yield values (Φ_P) were determined by a method based on the one developed by de Mello *et al.*,[37] as described elsewhere.[13] The error was estimated to be about 20%.

Emission decay curves of dilute DCM solutions (Abs at $\lambda_{ex} < 0.1$) were recorded using the time-correlated single-photon counting method (TCSPC) on a Fluorolog 3-2(iHR320) spectrofluorimeter equipped with a nanoled-370 (λ_{ex}=371 nm). Emitted photons were detected at 90° through a monochromator by means of a Hamamatsu R928 photomultiplier. Emission was recorded near the maximum with a bandpass of 10-15 nm. The instrumental response was recorded directly on the sample at 626 nm before each decay curve. All analyzes were recorded using the Datastation v2.7 software. The decay curves were analyzed with reconvolution and global non-linear least-squares minimization method using DAS6 v6.8 software.

For photochemistry, non-degassed dilute dye solutions were placed in fluorescence 1 cm × 1cm quartz cuvettes and irradiated in a Rayonet reactor equipped with lamps emitting at 350 nm.

Computational details. The ORCA software was employed for all calculations (the geometry optimization, the ground-state and excited-state electronic structures, and optical spectra) with the aid of the Gabedit visualization program .[38] Density functional theory (DFT) and time-dependent DFT (TD-DFT) calculations were performed with the PBE0 functional.[39] The ground state

(S_0) and the lowest triplet state (T_1) geometries of compounds were fully optimized with the DFT method using the Perdew-Burke-Ernzerhof PBE0 functional without symmetry constraints.[40] In all calculations, the "double-ζ" quality basis set LANL2DZ with Hay and Wadt's relative effective core potential ECP (outer-core [($5s^2 5p^6$)] electrons and the ($5d^6$) valence electrons)[41] was employed for the Re atom. The solvent effect (DCM, ε = 9.08) was simulated using the Conductor-like Polarizable Continuum Model (CPCM).[42]The vibrational frequencies calculations were performed using the optimized structural parameters of compounds, to confirm that each optimized structure represents a local minimum on the potential energy surface. On the basis of the optimized ground state geometry, the absorption properties were calculated by the TD-DFT method at the PBE0/LANL2DZ level. The emission has been calculated by DFT considering the difference of energy between the optimized triplet state and the singlet state at the same geometry.

Conflicts of interest

There are no conflicts to declare.

Electronic Supplementary Information

Experimental details including molecular views, and CIF data; additional computational, electrochemical and spectroscopic data; proton numbering and NMR spectra of compounds **1–3**.

Acknowledgements

We thank Mr. Nicolas Ratel-Ramond (CEMES-CNRS) for the measurement of powder XRD patterns, Dr. Charles-Louis Serpentini (IMRCP) for the measurement of emission lifetimes, Ms. Marie Goizet (ENSIACET) for the study of photochemical stability, as well as Dr. Alix Sournia-Saquet and Mr. Alain Moreau (LCC) for the electrochemical measurements.

REFERENCES

1 V. Sathish, A. Ramdass, P. Thanasekaran, K.-L. Lu and S. Rajagopal, *J. Photochem. Photobiol. C*, **2015**, *23*, 25–44. L. Ravotto and P. Ceroni, *Coord. Chem. Rev.*, **2017**, *346*, 62–76. P. Alam, C. Climent, P. Alemany and I. R. Laskar, *J. Photochem. Photobiol. C*, **2019**, *41*, 100317.

2 K. Choroba, A. Maroń, A. Świtlicka, A. Szłapa-Kula, M. Siwy, J. Grzelak, S. Maćkowski, T. Pedzinski, E. Schab-Balcerzak and B. Machura, *Dalton Trans.*, **2021**, *50*, 3943–3958. A. M. Maroń, A. Szlapa-Kula, M. Matussek, R. Kruszynski, M. Siwy, H. Janeczek, J. Grzelak, S. Maćkowski, E. Schab-Balcerzak and B. Machura, *Dalton Trans.*, **2020**, *49*, 4441–4453. T. Klemens, A. Świtlicka-Olszewska, B. Machura, M. Grucela, H. Janeczek, E. Schab-Balcerzak, A. Szlapa, S. Kula, S. Krompiec, K. Smolarek, D. Kowalska, S. Mackowski, K. Erfurt and P. Lodowski, *RSC Adv.*, **2016**, *6*, 56335–56352. A. Świtlicka, T. Klemens, B. Machura, E. Schab-Balcerzak, K. Laba, M. Lapkowski, M. Grucela, J. Nycz, M. Szala and M. Kania, *RSC Adv.*, **2016**, *6*, 112908–112918. T. Klemens, A. Switlicka, B. Machura, S. Kula, S. Krompiec, K. Łaba, M. Korzec, M. Siwy, H. Janeczek, E. Schab-Balcerzak, M. Szalkowski, J. Grzelak and S. Maćkowski, *Dyes Pigm.*, **2019**, *163*, 86–101. T. Klemens, A. Świtlicka-Olszewska, B. Machura, M. Grucela, E. Schab-Balcerzak, K. Smolarek, S. Mackowski, A. Szlapa, S. Kula, S. Krompiec, P. Lodowski and A. Chrobok, *Dalton Trans.*, **2016**, *45*, 1746–1762. T. Klemens, K. Czerwińska, A. Szlapa-Kula, S. Kula, A. Świtlicka, S. Kotowicz, M. Siwy, K. Bednarczyk, S.

Krompiec, K. Smolarek, S. Maćkowski, W. Danikiewicz, E. Schab-Balcerzak and B. Machura, *Dalton Trans*., **2017**, *46*, 9605–9620.

3 M. V. Werrett, G. S. Huff, S. Muzzioli, V. Fiorini, S. Zacchini, B. W. Skelton, A. Maggiore, J. M. Malicka, M. Cocchi, K. C. Gordon, S. Stagni and M. Massi, *Dalton Trans.*, **2015**, *44*, 8379–8393. G.-W. Zhao, J.-H. Zhao, Y.-X. Hu, D.-Y. Zhang and X. Li, *Synth. Met.*, **2016**, *212*, 131–141. Y.-X. Hu, G.-W. Zhao, Y. Dong, Y.-L. Lü, X. Li and D.-Y. Zhang, *Dyes Pigm*., **2017**, *137*, 569–575.

4 V. Komreddy, K. Ensz, H. Nguyen and D. P. Rillema, *Inorg. Chim. Acta*, **2020**, *511*, 119815. L. Veronese, E. Quartapelle Procopio, T. Moehl, M. Panigati, K. Nonomura and A. Hagfeldt, *Phys. Chem. Chem. Phys*., **2019**, *21*, 7534–7543. X. Ji, P. Zhang, W. Wei, H. Zhang and B. Xia, *J. Organomet. Chem.*, **2018**, *862*, 40–52.

5 Y. Kuramochi, O. Ishitani and H. Ishida, *Coord. Chem. Rev.*, **2018**, *373*, 333–356.

6 M. Y. Petyuk, A. S. Berezin, A. L. Gushchin, I. Yu. Bagryanskaya, A. Yu. Baranov and A. V. Artem'ev, *Inorg. Chim. Acta*, **2021**, *516*, 120136. M. Yu. Petyuk, A. S. Berezin, I. Yu. Bagryanskaya, O. I. Artyushin, V. K. Brel and A. V. Artem'ev, *Inorg. Chem. Commun*., **2020**, *119*, 108058.

7 G.-X. Jin, T. Wang, Y. Sun, Y.-L. Li and J.-P. Ma *Inorg. Chem*., **2020**, *59*, 15019-15027.

8 E. Quartapelle Procopio, M. Mauro, M. Panigati, D. Donghi, P. Mercandelli, A. Sironi, G. D'Alfonso and L. De Cola, *J. Am. Chem. Soc.*, **2010**, *132*, 14397–14399.

9 V. Sathish, A. Ramdass, Z.-Z. Lu, M. Velayudham, P. Thanasekaran, K.-L. Lu and S. Rajagopal, *J. Phys. Chem. B*, **2013**, *117*, 14358−14366. B. Manimaran, P. Thanasekaran, T. Rajendran, R.-J. Lin, I.-J. Chang, G.-H. Lee, S.-M. Peng, S. Rajagopal and K.-L. Lu, *Inorg. Chem.*, **2002**, *41*, 5323–5325. Y.-J. Pu, R. E. Harding, S. G. Stevenson, E. B. Namdas, C. Tedeschi, J. P. J. Markham, R. J. Rummings, P. L. Burn and I. D. W. Samuel, *J. Mater. Chem.*, **2007**, *17*, 4255–4264.

10 Z. Wang, Y. Wang, Y. Xu, J. Li, X. Ke, C. Jia, Z. Si, Y. Wan and Q. Duan, *Opt. Mater.*, **2020**, 105, 109876.

11 Q. Wei, Y. Dai, C. Chen, L. Shi, Z. Si, Y. Wan, Q. Zuo, D. Han and Q. Duan, *J. Mol. Struct.*, **2018**, 1171, 786–792. M. T. Gabr and F. C. Pigge, *Dalton Trans.*, **2017**, *46*, 15040–15047. T. Tao, H. Fang, Y.-X. Peng, M.-D. Zhang and W. Huang, *Inorg. Chem. Commun.*, **2017**, *84*, 15–19.

12 J. Wang, B. Delavaux-Nicot, M. Wolff, S. Mallet-Ladeira, R. Métivier, E. Benoist and S. Fery-Forgues, *Dalton Trans.*, **2018**, *47*, 8087–8099.

13 J. Wang, A. Poirot, B. Delavaux-Nicot, M. Wolff, S. Mallet-Ladeira, J. P. Calupitan, C. Allain, E. Benoist and S. Fery-Forgues, *Dalton Trans*., **2019**, *48*, 15906–15916.

14 J. P. Calupitan, A. Poirot, J. Wang, B. Delavaux-Nicot, M. Wolff, M. Jaworska, R. Métivier, E. Benoist, C. Allain and S. Fery-Forgues, *Chem. Eur. J.*, **2021**, *27*, 4191−4196.

15 P. Bisel, L. Al-Momanib and M. Müller, *Org. Biomol. Chem.*, **2008**, *6*, 2655−2665.

16 J. Liu, D. Obando, V. Liao, T. Lifa, R. Codd, *Eur. J. Med. Chem.*, **2011**, *46*, 1949−1963. K. Spilovska, F. Zemek, J. Korabecny, E. Nepovimova, O. Soukup, M. Windisch and K. Kuca, Curr. Med. Chem., **2016**, *23*, 3245−3266.

17 Y.-X. Li, H. Zhang, M.-N. Yu, S.-S. Wang, Y.-R. Liu, D.-Q. Lin, L.-H. Xie, Z.-Q. Lin and W. Huang, *Nanoscale*, **2019**, *11*, 5158–5162.

18 L. Zhang, J. Liu, J. Gao, R. Lu and F. Liu, *RSC Adv.*, **2017**, *7*, 46354–46357. M.-M. Shi, V.C. Tung, J.-J. Nie, H.-Z. Chen and Y. Yang, *Org. Electron.*, **2014**, *15*, 281–285.

19 C. Ainsworth, *J. Am. Chem. Soc.*, **1955**, *77*, 1148−1150.

20 Z. Geng, Y. Lu, S. Zhang, X. Jiang, P. Huo, J. Luan and G. Wang, *Polym. Int*., **2014**, *63*, 333−337.

21 J. Lincke, D. Lässig, K. Stein, J. Moellmer, A. V. Kuttatheyil, C. Reichenbach, A. Moeller, R. Staudt, G. Kalies, M. Bertmer and H. Krautscheid, *Dalton Trans.*, **2012**, *41*, 817−824.

22 L. Suntrup, S. Klenk, J. Klein, S. Sobottka and B. Sarkar, *Inorg. Chem.*, **2017**, *56*, 5771−5783.

23 R. Eychenne, S. Guizani, J.- H. Wang, C. Picard, N. Malek, P.-L. Fabre, M. Wolff, B. Machura, N. Saffon, N. Lepareur and E. Benoist, *Eur. J. Inorg. Chem*., **2017**, *1*, 69–81. T. Y. Kim, A. B. S. Elliott, K. J. Shaffer, C. J. McAdam, K. C. Gordon and J. D. Crowley, *Polyhedron*, **2013**, *52*, 1391–1398.

24 W. K. C. Lo, G. S. Huff, J. R. Cubanski, A. D. W. Kennedy, C. J. McAdam, D. A. McMorran, K. C. Gordon and J. D. Crowley, *Inorg. Chem.*, **2015**, *54*, 1572–1587. P. Datta, D. Sarkar, A. P. Mukhopadhyay, E. Lopez-Torrez, C. J. Pastor and C. Sinha, *J. Organomet. Chem*., **2011**, *696*, 488–495.

25 Y. Zhou, J. W. Kim, R. Nandhakumar, M. J. Kim, E. Cho, Y. S. Kim, Y. H. Jang, C. Lee, S. Han, K. M. Kim, J.-J. Kim and J. Yoon, *Chem. Commun*., **2010**, *46*, 6512–6514 and references therein. G. V. Loukova, *Chem. Phys. Lett*., **2002**, *353*, 244–252.

26 S. Sato and O. Ishitani, *Coord. Chem. Rev.* **2015**, *282–283*, 50–59. A. Vlček, *Top. Organomet. Chem.* **2010**, *29*, 73-114.

27 C. Carayon and S. Fery-Forgues, *Photochem. Photobiol. Sci.*, **2017**, *16*, 1020−1035 and refs cited therein.

28 J. Gierschner, J. Shi, B. Milián-Medina, D. Roca-Sanjuán, S. Varghese and S. Y. Park, *Adv. Optical Mater.*, **2021**, 2002251.

29 D. Barman, R. Gogoi, K. Narang and P. K. Iyer, *Front. Chem.*, **2020**, *8*, 483. Y. Sagara, S. Yamane, M. Mitani, C. Weder and T. Kato, *Adv. Mater.*, **2016**, *28*, 1073–1095. Z. Ma, Z. Wang, M. Teng, Z. Xu and X. Jia, *ChemPhysChem*, **2016**, *16*, 1811–1828. C. Wang and Z. Li, *Mater. Chem. Front.*, **2017**, *1*, 2174–2194.

30 L. Wilbraham, M. Louis, D. Alberga, A. Brosseau, R. Guillot, F. Ito, F. Labat, R. Métivier, C. Allain and I. Ciofini, *Adv. Mater.*, **2018**, *30*, 1800817.

31 S. Mu, K. Oniwa, T. Jin, N. Asao, M. Yamashita and S. Takaishi, *Org. Electron.*, **2016**, *34*, 23–27. H.-H. Fang, J. Yang, J. Feng, T. Yamao, S. Hotta and H.-B. Sun, *Laser Photonics Rev.*, **2014**, *8*, 687–715. S. Hotta and M. Goto, *Adv. Mater*., **2002**, *14*, 498–501. Z. Lu, Y. Zhang, H. Liu, K. Ye, W. Liu and H. Zhang, *Angew. Chem. Int. Ed.*, **2020**, *59*, 4299–4303.

32 H. Liu, Z. Bian, Q. Cheng, L. Lan, Y. Wang and H. Zhang, *Chem. Sci*., **2019**, *10*, 227–232. Z.-F. Liu, X. Chen and W. J. Jin, *J. Mater. Chem. C*, **2020**, *8*, 7330–7335.

33 SADABS, Program for data correction, Bruker-AXS.

34 G. M. Sheldrick, *Acta Cryst. A*, **2015**, *71*, 3–8.

35 G. M. Sheldrick, *Acta Cryst. C*, **2015**, *71*, 3–8.

36 K. Suzuki, A. Kobayashi, S. Kaneko, K. Takehira, T. Yoshihara, H. Ishida, Y. Shiina, S. Oishi and S. Tobita, *Phys. Chem. Chem. Phys*., **2009**, *11*, 9850–9860.

37 J. C. De Mello, H. F. Wittmann and R. H. Friend, *Adv. Mater.*, **1997**, *9*, 230–232.

38 A.-R. Allouche, *J. Comput. Chem.*, **2011**, *32*, 174–182.

39 C. Adamo, V. Barone, *J. Chem. Phys.* **1999**,*110*, 6158–6170.

40 J. P. Perdew, K. Burke, M. Ernzerhof, *Phys. Rev. Lett.* **1996**, *77*, 3865–3868.

41 P. J. Hay, W. R. Wadt, *J. Chem. Phys.* **1985**, *82*, 270–283; b) P. J. Hay, W. R. Wadt, *J. Chem. Phys.* **1985**, *82*, 299–310.

42 B. Mennucci, J. Tomasi, *J. Chem. Phys.* **1997**, *106*, 5151–2158. M. Cossi, V. Barone, B. Mennucci, J. Tomasi, *Chem. Phys. Lett.* **1998**, *286*, 253–260.